

# Effect of Mo content on the structural and physical properties of $\text{Cr}_{100-x}\text{Mo}_x$ alloys

**Abstract.** Alloying Cr with Mo, which is isoelectric with it, shows an unexpected decrease in the Néel temperature ( $T_N$ ) with an increase in Mo concentration. This is attributed to a delocalization of the 3-d bands in Cr through the introduction of 4-d electrons of Mo. In the present investigation the effect of Mo concentration on the structural, magnetic and electrical properties of Cr is systematically studied. A series of  $\text{Cr}_{100-x}\text{Mo}_x$  alloys, with  $x = 0, 3, 7, 15$  and  $25$ , was prepared and the actual concentrations established using electron microprobe analyses. XRD studies confirm the bcc structure of these alloys as in pure Cr and indicate an increase in lattice constant with an increase in Mo concentration. The crystallite sizes calculated from these results for the  $\text{Cr}_{100-x}\text{Mo}_x$  alloys ranges between 15 and 30 nm. The physical properties of these alloys were investigated through magnetic susceptibility ( $\chi$ ), Seebeck coefficient ( $S$ ), electrical resistivity ( $\rho$ ) and Hall coefficient ( $R_H$ ) as function of temperature ( $T$ ) measurements.  $T_N$  values obtained from these measurements are comparable.

## 1. Introduction

Chromium is a fascinating metal to study because of its antiferromagnetic spin-density-wave (SDW) behaviour below 311 K [1]. The SDW results from the ‘nesting’ of the electron and hole sheets of the Fermi surface on cooling through the Néel temperature ( $T_N$ ) [2, 3]. This nesting effect is sensitive to changes in the electron-to-atom ( $e/a$ ) ratio and is influenced by the diluent elements used to dope Cr. In pure Cr, the periodicity of the SDW is incommensurate (I) with that of the lattice [1].

Chromium has six valence electrons and therefore its  $e/a$  ratio is 6. When it is alloyed with an element having  $e/a$  greater than 6,  $T_N$  increases with concentration and ordering changes to commensurate (C) [1]. This happens because the addition of electrons to the d-band of Cr enlarges the electron Fermi surface and brings to match with hole Fermi surface. This results in a larger nesting area,  $T_N$  then increases and the ordering becomes commensurate. In opposite case i.e. for  $e/a$  less than 6,  $T_N$  decreases and the magnetic state remains incommensurate, as in pure Cr. In this case the electron Fermi surface shrinks. There is a mismatch between the electron and hole Fermi surfaces causing  $T_N$  to decrease [1, 2, 4]. Few reports are available on Cr alloys in which the diluent elements have the same  $e/a$  values as in pure Cr [1]. Considering this, investigations into the physical properties of Cr alloys with isoelectronic elements are important, as it rules out the effect of  $e/a$  on the Fermi surface. [5].

The dependence of  $T_N$  on the electron concentration and nature of the solute atoms were described by Fedders and Martins [6], and Koehler *et al.* [7] with the help of the isotropic model in which two spherical pieces of Fermi surface with a radius  $k_c$  in different bands are connected by a wave vector  $q$ . They showed that  $T_N$  for such a model is given by an equation [6],  $T_N = T_0 \exp(-1/\lambda)$ , where  $T_0$  is a function which depends on the band structure and  $\lambda = \gamma^2 V(0) k_c^2 / 2\pi^2 v$ , where  $\gamma$  is a mean overlap

matrix element for electrons in the same band,  $V(0)$  is the average screened Coulomb potential and  $v$  is the arithmetic mean of the Fermi velocities in the two bands. The addition of Mo or W slightly modifies the Fermi surface, but since the d-wave functions in these elements are less localized than those in pure Cr, the value of  $\gamma$  is reduced and  $T_N$  falls with diluent concentration [1, 6, 7].

$\text{Cr}_{100-x}\text{Mo}_x$  alloys with Mo concentrations below 25 at.% were studied previously by several researchers [5, 10, 11, 12]. Mamiya *et al.* [5] reported extensive measurements on the electrical resistivity and low temperature specific heat for the  $\text{Cr}_{100-x}\text{Mo}_x$  alloys in the range  $0 \leq x \leq 36.6$  and determined the Néel temperatures from the positions of the anomalies. Mitchell *et al.* [8] compared the effect of Mo and Fe addition to Cr on  $T_N$  by measuring the electrical resistivity of Cr-Mo and Cr-Fe alloys, while the thermoelectric power studies for the  $\text{Cr}_{100-x}\text{Mo}_x$  alloys with  $x = 0, 5, 10$  and  $x \geq 25$  were reported by Schröder and Tomaschke [9]. It was found that  $\text{Cr}_{100-x}\text{Mo}_x$  alloys with  $x \geq 25$  are paramagnetic. The effect of the type and concentration of solute atoms on transport properties of antiferromagnetic Cr alloys have been studied by Trego and Mackintosh [10] through electrical resistivity and thermoelectric power measurements. This study reported measurements for the  $\text{Cr}_{100-x}\text{Mo}_x$  alloys with Mo concentration up to approximately 21 at.%. The magnetic susceptibility and Hall coefficient measurements were reported by Bender *et al.* [11] and Shabel *et al.* [12], respectively. However, the Hall coefficient measurements reported were only for the paramagnetic Cr-Mo alloys [12]. Mo was doped to form ternary alloys in order to study two interesting binary Cr alloys SDW systems [1, 13, 14]. The interesting behaviours in Cr-Al-Mo [13] and Cr-Si-Mo [14] ternary alloy systems might be related to the Mo in these and the need to understand the fundamental behaviour of Cr-Mo alloys better therefore arise. This study focus on measurements done using newly sophisticated instruments and extend existing knowledge to include more physical and structural properties of this  $\text{Cr}_{100-x}\text{Mo}_x$  alloys, with  $x = 0, 3, 7, 15, 25$ .

## 2. Experimental

The  $\text{Cr}_{100-x}\text{Mo}_x$  alloys, with  $x = 0, 3, 7, 15$  and  $25$ , were prepared by arc melting in a purified low pressure argon atmosphere. The precursors used for the preparation of these binary alloys were Cr and Mo with purities 99.999% and 99.99%, respectively. Cr and Mo were weighed in required proportion and melted together into a button form in an arc melting furnace with argon atmosphere. After etching the samples with hydrochloric acid they were each sealed in a quartz ampoule filled with pure argon gas at low pressure and annealed at 1273 K for seven days and then quenched in ice bath. The prepared alloy samples were cut and polished using spark erosion techniques in preparation for their characterization.

Structural studies of these samples were carried out by XRD (Phillips PAN analytical X-pert Pro X-ray diffractometer) in the  $2\theta$  geometry, in the range  $10\text{--}90^\circ$  using a  $\text{Cu-K}\alpha_1$  radiation ( $\lambda = 1.54056\text{\AA}$ ). The XRD patterns were compared with standard Joint Council of Powder Diffraction Database (JCPDD) files of Cr (04-008-5987) and Mo (42-1120). In order to determine actual composition of the samples, microprobe analyses were carried out using a JEOL electron microprobe analyzer (EPMA) model JXA-8900. A Quantum Design (QD) Physical Property Measurement System (PPMS) incorporating appropriate measuring options was used for the electrical resistivity ( $\rho$ ) and Seebeck coefficient ( $S$ ) measurements in the temperature range 2 K to 350 K. Magnetic susceptibility measurements in the temperature range 2 K to 350 K were performed using a QD Magnetic Properties Measurement System (MPMS).

## 3. Results and Discussion

XRD patterns for the  $\text{Cr}_{100-x}\text{Mo}_x$  alloy system with  $x = 0, 7$  and  $25$  are shown in figure 1(a). These patterns confirm the phase synthesis of alloys with expected body centred cubic (bcc) crystal structure. The lattice parameters were computed from the XRD patterns for all the alloys. It is observed that lattice parameter increases with Mo content as shown in figure 1(b). The crystallite sizes were calculated by using Debye Scherrer's formula [15]:

$$D = \frac{0.9 \lambda}{\beta \cos \theta}, \quad (1)$$

where  $D$  is crystallite size,  $\lambda$  is the wavelength of the source,  $\beta$  is the full width at half maximum (FWHM) of the peak and  $\theta$  corresponds to the Bragg angle. The calculated crystallite sizes for these  $\text{Cr}_{100-x}\text{Mo}_x$  alloys ranges between 15 and 30 nm.

Electron microprobe analyses done on the  $\text{Cr}_{100-x}\text{Mo}_x$  alloys show that all the samples have a uniform composition and the results are tabulated in table 1. Differences in the nominal and actual concentrations are attributed to weight loss during crushing and to evaporation of Cr during melting [5]. The bright and dark spots are observed in the backscattered SEM images shown in figure 2 (a) and (b), and the corresponding Cr and Mo concentrations for bright and dark spots are tabulated in table 1. Also the black spots are observed in SEM images were analysed, these are attributed to the presence of Cr oxide in some regions of the alloys. The area covered by the black spots indicates that the percentage of Cr oxide is approximately 1% to 5% and this should not affect the antiferromagnetic properties of the present alloy system. As far as can be ascertained this is the first report on the correlation between microprobe and SEM analysis for Cr-Mo alloys.

Figure 3 shows the electrical resistivity measurements as a function of temperature,  $\rho(T)$ , for the series of  $\text{Cr}_{100-x}\text{Mo}_x$  alloys with  $x \leq 15$ . These curves show well defined anomalies in the form of clear minimum followed by hump in the  $\rho(T)$  curves. The anomaly, which occurs in the vicinity of  $T_N$  is monotonically depressed with increasing Mo concentration as discussed by Mamiya *et al.* [5]. From previous measurements it is known that  $\text{Cr}_{100-x}\text{Mo}_x$  alloys with  $x \geq 25$  are paramagnetic [5].

$T_N$  values were obtained from  $d\rho/dT$  versus  $T$  curves by taking the temperature associated with the minimum in these curves [1, 14]. The inset of figure 3 shows  $d\rho/dT$  versus  $T$  for the  $\text{Cr}_{85}\text{Mo}_{15}$  alloy as an example. The increase in the electrical resistivity below  $T_N$  for Cr-Mo alloys is attributed to an opening up of the SDW energy gap over part of the Fermi surface [1, 5, 8, 16]. Mamiya *et al.* [5] and Trego *et al.* [10] published some resistivity studies on different  $\text{Cr}_{100-x}\text{Mo}_x$  alloys, but no resistivity studies were previously reported for the particular alloys investigated in the present study.

The thermoelectric power is an essential tool for determining  $T_N$  in Cr and its alloys because it is more sensitive as compared to the electrical resistivity, to changes in electronic band structure when the SDW state is entered on cooling through  $T_N$  [1]. Previously Schröder *et al.* [9] reported thermoelectric measurements for the Cr-Mo alloys in the temperature range 100 K to 600 K while the present study gives the thermoelectric measurements for Cr-Mo alloys in the temperature range 2 K to 400 K. Figure 4 depicts the  $S(T)$  curves of pure Cr and  $\text{Cr}_{100-x}\text{Mo}_x$  alloys with  $x = 3, 7, 15$  and 25. The experimental  $S(T)$  curves show a prominent dome, just below  $T_N$ , also ascribed to the influence of the SDW energy gap [1, 10, 17]. From figure 4, it is seen that with an increase in Mo concentration in the

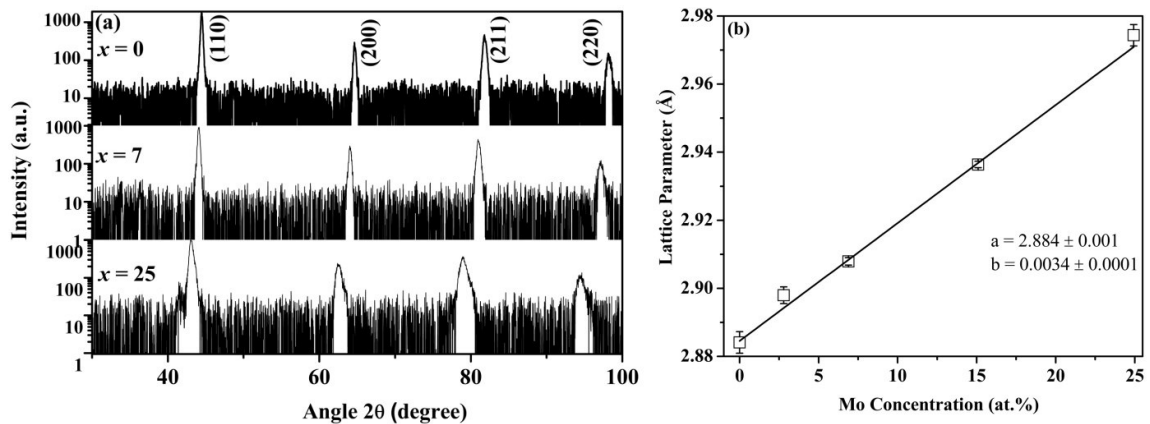


**Figure 1.** (a) The XRD patterns for the  $\text{Cr}_{100-x}\text{Mo}_x$  alloys, with  $x = 0, 7$  and 25 (b) The variation in the lattice parameter with Mo content.

**Table 1.** Elemental concentrations obtained from electron microprobe analyses for Cr-Mo alloys.

Sr. No.	Name of the sample	Nominal concentration (at.%)		Actual concentration (Microprobe) (at.%)		Bright Region		Dark Region	
		Cr	Mo	Cr	Mo	Cr	Mo	Cr	Mo
1	Cr <sub>97</sub> Mo <sub>3</sub>	97	3	97.0 ± 0.2	2.8 ± 0.2	97.27 ± 0.04	2.72 ± 0.03	97.30 ± 0.07	2.70 ± 0.07
2	Cr <sub>93</sub> Mo <sub>7</sub>	93	7	93.1 ± 0.6	6.9 ± 0.6	93.0 ± 0.2	7.05 ± 0.15	98.8 ± 0.8	1.2 ± 0.8
3	Cr <sub>85</sub> Mo <sub>15</sub>	85	15	84.9 ± 0.6	15.1 ± 0.6	83.3 ± 0.4	16.4 ± 0.4	86.6 ± 0.6	13.4 ± 0.6
4	Cr <sub>75</sub> Mo <sub>25</sub>	75	25	74 ± 1	26 ± 1	71.2 ± 0.3	28.8 ± 0.3	79 ± 1	21 ± 1

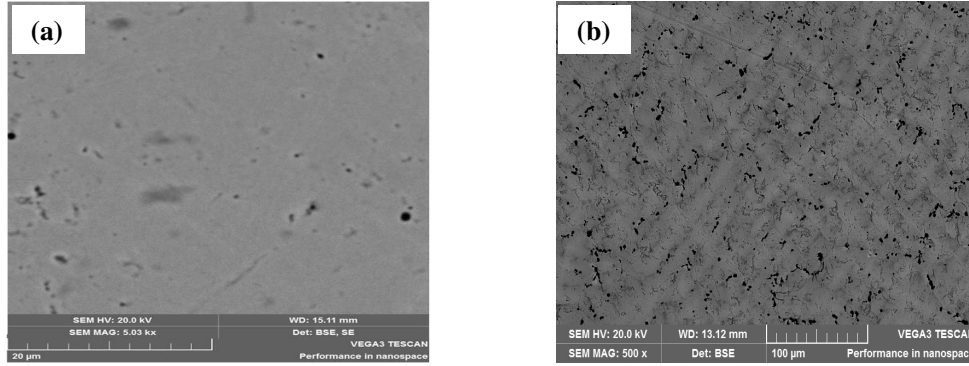


**Figure 2.** Backscattered SEM images of Cr<sub>100-x</sub>Mo<sub>x</sub> alloys with (a)  $x = 3$  and (b)  $x = 25$ .

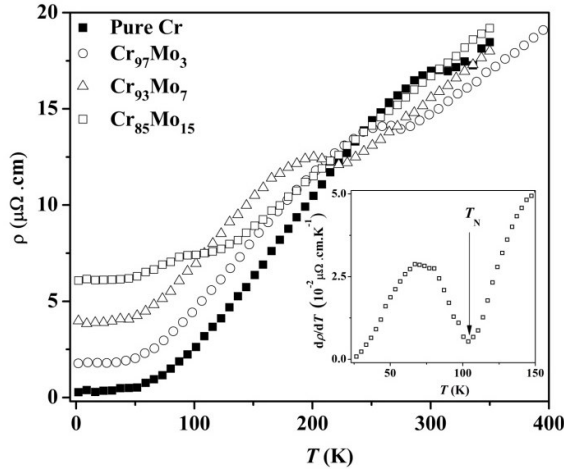


**Figure 3.** Electrical resistivity ( $\rho$ ) as a function of temperature ( $T$ ) for the Cr<sub>100-x</sub>Mo<sub>x</sub> alloys. Inset shows  $d\rho/dT$  versus  $T$  for Cr<sub>85</sub>Mo<sub>15</sub> alloy.

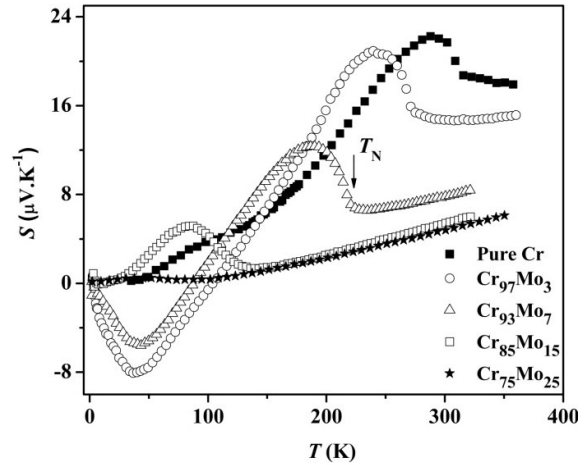


**Figure 4.** The Seebeck coefficient ( $S$ ) as a function of temperature ( $T$ ) for Cr<sub>100-x</sub>Mo<sub>x</sub> alloys.

Cr-Mo alloys, the dome is depressed and almost vanishes for sample with 25 at.% Mo. The  $T_N$  values were determined from the temperature at the minimum point on the  $dS/dT$  versus  $T$  curve [17]. For the Cr<sub>100-x</sub>Mo<sub>x</sub> alloys with  $x = 3$  and 7, the valleys are observed below  $T_N$ , this can be attributed to phonon or magnon drag terms [10, 18].

The dependence of  $T_N$  as obtained from  $\rho(T)$  and  $S(T)$  measurements on Mo concentration is shown in figure 5.  $T_N$  decreases linearly with an increase in Mo concentration and disappears for an alloy with

25 at.% Mo. These results agree very well with results obtained in ref. [5]. In addition, the  $T_N$  values determined from resistivity and thermoelectric measurements are comparable with each other.

Magnetic susceptibility ( $\chi$ ) measurements as a function of temperature for pure Cr and the  $\text{Cr}_{97}\text{Mo}_3$  alloy are shown in figure 6(a) and (b), respectively. The arrows in the  $\chi(T)$  curves show the positions of  $T_N$  obtained from  $\rho(T)$  and  $S(T)$  measurements. Pure Cr (figure 6(a)) shows a sharp change in slope of the  $\chi(T)$  curve on heating through  $T_N$ .  $\chi(T)$  for pure Cr is distinctly depressed at  $T < T_N$ , and is attributed to the effects of the SDW energy gap. A discontinuous sharp step down is observed in the  $\chi(T)$  curve of pure Cr at  $T_{\text{sf}} \approx 123$  K where a spin-flip transition occurs. At  $T_{\text{sf}}$  the transverse (T) ISDW phase transforms on cooling to a longitudinal (L) ISDW phase [1, 17]. Figure 6(b) shows the increase in  $\chi(T)$  on cooling from 350 K to  $T_N$  giving a maximum value for  $\chi$  at  $T_N$ , followed by a sharp (or sudden, choose) decrease on further cooling below  $T_N$ . This results in an anomalous sharp peak near  $T_N$ . Sousa *et al.* [19] observed a similar behaviour in the  $\text{Cr}_{100-x}\text{Al}_x$  alloy system with  $x = 2.23$  and 2.83. They attributed the peaks in  $\chi$  at  $T_N$  to a local moments resulting in Curie-Weiss paramagnetism above  $T_N$  [1, 19]. At  $T \approx 65$  K there appears to be a spin-flip transition, not previously reported.

Figure 7 shows the  $R_H(T)$  curves for pure Cr and the  $\text{Cr}_{97}\text{Mo}_3$  alloy, respectively. The  $R_H(T)$  behaviour for pure Cr well matches that reported in [17, 20, 21]. The prominent upturn in  $R_H(T)$  in Cr alloys at  $T < T_N$  is attributed to the formation of the SDW energy gap, while the downturn below about 150 K probably reveals the spin-flip transition at  $T_{\text{sf}} = 123$  K. In  $R_H(T)$  curve for the  $\text{Cr}_{97}\text{Mo}_3$  alloy, it is observed that on cooling through  $T_N$ , there is a rise in  $R_H$  values. At  $T \approx 200$  K the  $R_H$  values decrease

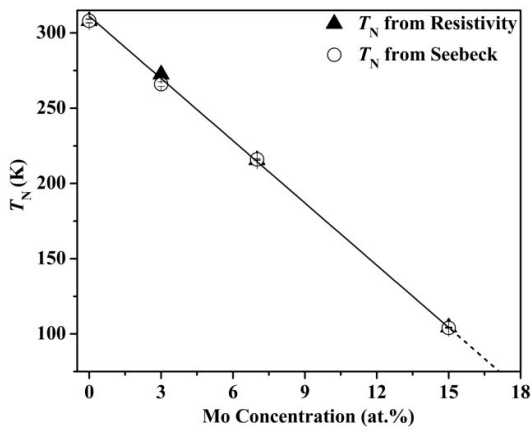


**Figure 5.** Variation of Néel temperatures ( $T_N$ ) with respect to Mo content in  $\text{Cr}_{100-x}\text{Mo}_x$  alloys.

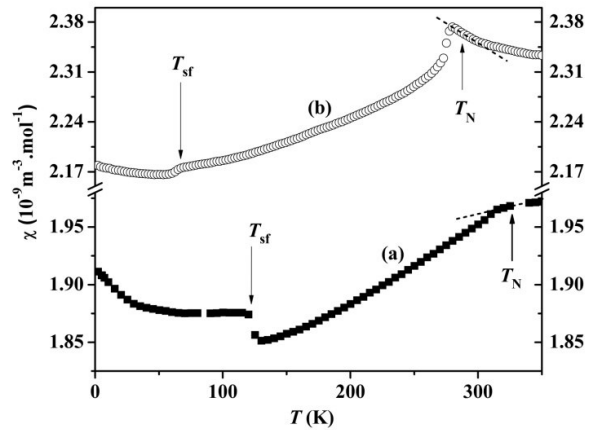


**Figure 6.** The magnetic susceptibility ( $\chi$ ) as function of temperature ( $T$ ) for the  $\text{Cr}_{100-x}\text{Mo}_x$  with (a)  $x = 0$  and (b)  $x = 3$ .

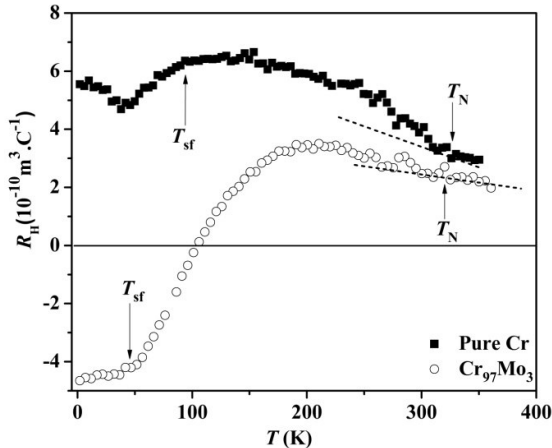


**Figure 7.** The Hall coefficient ( $R_H$ ) as a function of temperature ( $T$ ) for the pure Cr and  $\text{Cr}_{97}\text{Mo}_3$  alloy. Arrows indicate the Néel temperatures ( $T_N$ ) and the spin-flip transition temperature  $T_{\text{sf}}$ .

monotonically and become negative at  $T \leq 100$  K. This behavior can be attributed to a change in the type of charge carriers below 100 K. The positive  $R_H$  indicates that the main charge carriers are holes and the hole mobility in the sample is greater than electron mobility [12].  $R_H$  values level off at  $T \approx 60$  K, corresponding to the temperature in  $\chi(T)$  curve for the same sample where a step is observed. This can possibly be attributed to a spin-flip transition, not previously reported in Cr-Mo alloys. Shabel *et al.* [12] reported the Hall effect measurements for Cr-Mo alloys in the concentration range  $x \geq 25$ . No Hall measurements were reported previously for the Cr-Mo alloys with  $x < 25$ .

#### 4. Conclusions

The present investigation reports on the  $\text{Cr}_{100-x}\text{Mo}_x$  alloys with  $x = 0, 3, 7, 15$  and  $25$ . The XRD results reveal the expected pure bcc structure of these alloys. The lattice parameters calculated from XRD patterns increase with Mo concentration. The crystallite sizes for the Cr-Mo alloys ranges from 15 to 30 nm. Prominent anomalies were observed in the electrical resistivity and Seebeck coefficient measurements as a function of temperature for these alloys.  $T_N$  values for each alloy, determined from these measurements agree very well with each other and decrease with an increase in Mo content.  $\chi(T)$  measurements give nearly same value for  $T_N$  and also indicate a spin-flip transitions in pure Cr and  $\text{Cr}_{97}\text{Mo}_3$  alloy. Hall measurements in  $\text{Cr}_{97}\text{Mo}_3$  alloys reported here for first time. It shows positive as well as negative  $R_H$  values, indicating a change in number as well as type of charge carriers.

#### Acknowledgements

Financial support from the South African NRF (Grant numbers 80928 and 80626) and the Faculty of Science from the University of Johannesburg are acknowledged.

#### References

- [1] Fawcett E, Alberts H L, Galkin V Y, Noakes D R and Yakhmi J V 1994 *Rev. Mod. Phys.* **66** 25
- [2] Lomer W M 1962 *Proc. Phys. Soc.* **80** 489
- [3] Ström-Olsen J O and Wilford D F 1980 *J. Phys. F: Metal Phys.* **10** 1467
- [4] Jayaraman A 1998 *Curr. Sci.* **75** (11) 1200
- [5] Mamiya T and Masuda Y 1976 *J. Phys. Soc. Jpn.* **40** (2) 390
- [6] Fedders P A and Martin P C 1966 *Phys. Rev.* **143** (1) 245
- [7] Koehler W C, Moon R M, Trego A L and Mackintosh A R 1966 *Phys. Rev.* **151**(2) 405
- [8] Mitchell M A and Goff J F 1972 *Phys. Rev. B* **5** (3) 1163
- [9] Schröder K and Tomaschke H 1968 *Phys. Kondens. Materie* **7** 318
- [10] Trego A L and Mackintosh 1968 *Phys. Rev.* **166** (2) 495
- [11] Bender D and Muller J 1970 *Phys. Kondens. Materie* **10** 342
- [12] Shabel B and Schröder K 1967 *J. Phys. Chem. Solids* **28** 2169
- [13] Muchono B, Prinsloo A R E, Sheppard C J, Alberts H L and Strydom A M 2014 *J. Magn. Magn. Mater.* **354** 222
- [14] Sheppard C J, Prinsloo A R E, Alberts H L, Strydom A M *J. Appl. Phys.* 2011 **109** 07E104-1
- [15] Cullity B D 1956 *Elements of X-ray diffraction Addison-Wesley Publ. Comp., Inc. U. S. America* 97
- [16] Mitchell M A and Goff J F 1975 *Phys. Rev. B* **12** (5) 1858
- [17] Sheppard C J, Prinsloo A R E, Alberts H L, Muchono B and Strydom A M 2014 *J. Alloys Compd.* **595** 164
- [18] Reddy L, Prinsloo A, Sheppard C and Strydom A 2013 *J. Korean Phys. Soc.* **63** (3) 756
- [19] Sousa J B, Amado M M, Pinto R P, Pinheiro M F, Braga M E, Moreira J M, Hedman L E, Åström H U, Khlaif L, Walker P, Garton G and Hukin D 1980 *J. Phys. F: Metal Phys.* **10** 2535
- [20] Furuya Y 1976 *J. Phys. Soc. Jpn.* **40** 490
- [21] Furuya Y, Misui T 1976 *J. Phys. Soc. Jpn.* **41** 1938